IEEE Access
Multidisciplinary ⋮ Rapid Review ⋮ Open Access Journal

Received January 17, 2022, accepted January 31, 2022, date of publication February 7, 2022, date of current version February 16, 2022.

Digital Object Identifier 10.1109/ACCESS.2022.3149311

24–40 GHz mmWave Down-Conversion Mixer With Broadband Capacitor-Tuned Coupled Resonators for 5G New Radio Cellular Applications

DONGGU LEE[1,2], (Student Member, IEEE), MYUNGHUN LEE[1,2,3], (Member, IEEE), BEOMYU PARK[1,2,3], (Member, IEEE), EUNJU SONG[1,2,4], (Student Member, IEEE), KYUDO LEE[1,2], (Student Member, IEEE), JEONGWOO LEE[5], (Member, IEEE), JUNGHWAN HAN[6], (Member, IEEE), AND KUDUCK KWON[1,2], (Senior Member, IEEE)

[1]Department of Electronics Engineering, Kangwon National University, Chuncheon 24341, South Korea
[2]Interdisciplinary Graduate Program in BIT Medical Convergence, Kangwon National University, Chuncheon 24341, South Korea
[3]Samsung Electronics Company Ltd., Hwaseong-si 18448, South Korea
[4]NICE Information Company Ltd., Seoul 07237, South Korea
[5]GCT Semiconductor Inc., Seoul 07071, South Korea
[6]Department of Radio and Information Communication Engineering, Chungnam National University, Daejeon 34134, South Korea

Corresponding author: Kuduck Kwon (kdkwon@kangwon.ac.kr)

This work was supported in part by GCT Semiconductor Inc.; in part by the Basic Science Research Program through the National Research Foundation of Korea (NRF) funded by the Ministry of Education under Grant NRF-2018R1D1A1B07042804; and in part by the Ministry of Science and ICT, South Korea, under the Information Technology Research Center Support Program supervised by the Institute for Information and Communications Technology Promotion (IITP) under Grant IITP-2021-2018-0-01433.

ABSTRACT In this paper, a 24–40 GHz broadband millimeter-wave (mmWave) down-conversion double-balanced mixer with a dual-band local oscillator (LO) buffer employing RF and IF coupled resonators is presented for 5G new radio (NR) frequency range 2 (FR2) cellular applications. The proposed mixer comprises a transformer-coupled g_m-boosted common-gate (CG) G_m-stage, a single-to-differential current-to-current RF capacitor-tuned coupled resonator, active switching stages with dual-band three-stage LO buffers, a current-to-voltage IF coupled resonator with gain equalization, and a wideband IF buffer with a transformer-based balun. The transformer-coupled g_m-boosted CG G_m-stage improves the NF and provides broadband input power matching. RF and IF coupled resonators enable an RF operating frequency range of 24–40 GHz and IF 1 dB bandwidth of more than 0.8 GHz, respectively. The implemented mixer was fabricated using a 40 nm CMOS process and characterized primarily in the 5G NR FR2 bands. The active die area was 0.654 mm^2, and the mixer drew a bias current of 16 mA from a nominal supply voltage of 1.1 V. The mixer exhibited an RF operating frequency range of 24–40 GHz, noise figure of 12.4 dB, conversion gain of 1.2 dB, IF 1 dB bandwidth of 1.1 GHz, and output-referred third-order intercept point of 6.8 dBm.

INDEX TERMS 5G, broadband, capacitor-tuned, cellular, coupled resonator, frequency range 2 (FR2), down-conversion mixer, dual-band, gain equalization, g_m-boosted, LO buffer, millimeter-wave (mmWave), new radio (NR).

I. INTRODUCTION

Fifth generation (5G) mobile communication technology, characterized by ultra-high speed, ultra-low latency, and hyper connection, makes it possible to realize key technologies of the fourth industrial revolution, such as smart factories, autonomous driving, and virtual/augmented reality. Several noncontiguous millimeter-wave (mmWave) frequency bands of n257, n258, n259, n260, and n261, located in the range of 24.25–43.5 GHz, are being allocated to different countries and regions for 5G new radio (NR) frequency range 2 (FR2) communications. Ultra-wideband mmWave phased array transceivers covering all the above bands are required to support frequency diversity and international roaming.

The associate editor coordinating the review of this manuscript and approving it for publication was Yiming Huo.

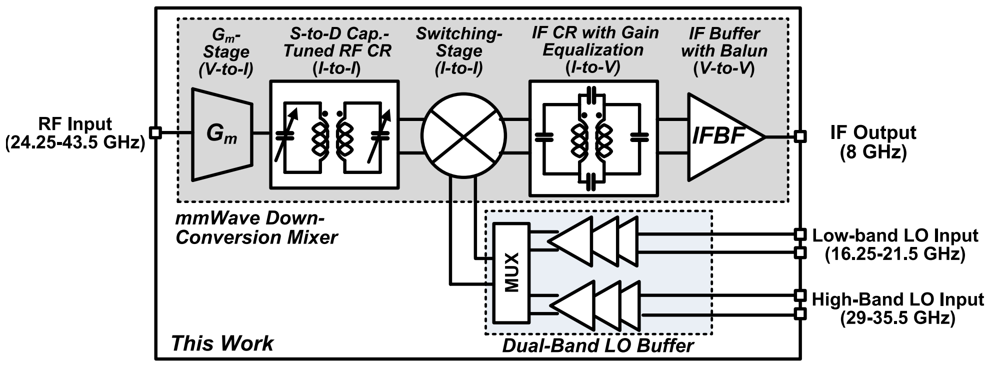

FIGURE 1. Block diagram of the proposed mmWave down-conversion mixer.

There are several 5G NR transceiver architecture options for user equipment such as RF, baseband (BB), and intermediate frequency (IF) interfaces [1]–[10]. The IF interface is the most realistic choice and widely employed in mobile platforms owing to the lower loss and ease of matching at the IF signal frequency [1], [3], [4], [6]–[9]. One chip solution, including 5G NR sub-6 GHz frequency range 1 (FR1) and mmWave IF transceiver, can also be used to implement low-cost and highly integrated IF interface option [4]. For a 5G NR mmWave transceiver with an IF ratio interface option to cover all the FR2 bands, a broadband down-conversion mixer is required.

mmWave down-conversion active mixers based on the conventional Gilbert-cell mixer are widely used in 5G NR FR2 applications. The authors of [2] and [3] employed a Gilbert mixer with current bleeding techniques in direct-conversion and sliding-IF receivers. Gilbert mixers with multiple gate transistors (MGTR) [11] or distributed derivative superposition (DS) [12] were introduced to improve linearity with low power. In addition, a 28 GHz bidirectional active mixer based on the Gilbert-cell topology was proposed to achieve both down- and up-conversion [13]. A K-band folded down-conversion double-balanced mixer based on the Gilbert-cell topology was also proposed to enhance the conversion gain and noise figure (NF) [14]. A 57–66 GHz down-conversion mixer employing the current-reused LO-boosting technique was presented to achieve a high conversion gain with a low LO input power [15]. A 20–26 GHz down-conversion mixer with a bleeding path G_m-boosting technique was presented in [16] to improve NF. The authors of [17] proposed a 79–110 GHz 4× quasi-subharmonic mixer to reduce the design burden of the phase shifter. A 57–66 GHz RF to 12 GHz IF down-conversion mixer employing output-matching, noise-and distortion-cancelling active balun was introduced in [18]. The active balun enhances the linearity performance of the mixer. A 57–66 GHz RF to 8.2-9.5 GHz IF down-conversion mixer with a transformer-based IF matching network was presented in [19]. The HBT transistors were used to improve performances. A new broadband down-conversion mixer topology with high performance is required to cover all the 5G NR FR2 bands.

In this paper, a 24–40 GHz broadband mmWave down-conversion double-balanced mixer is proposed for 5G NR FR2 cellular applications. To obtain broadband RF and IF characteristics, the G_m-stage of the mixer employs a transformer-coupled g_m-boosted common-gate (CG) topology with a single-to-differential (S-to-D) current-to-current (I-to-I) capacitor-tuned RF coupled resonator. The IF stage adopts a current-to-voltage (I-to-V) coupled resonator load with gain equalization and a wideband IF buffer stage with a differential-to-single (D-to-S) transformer-based balun. The remainder of this paper is organized as follows. Section II describes the proposed broadband mmWave down-conversion double-balanced mixer architecture. Section III elaborates on the circuit implementation of the mixer with a dual-band LO buffer. The experimental results are discussed in Section IV. The concluding remarks are presented in Section V.

II. PROPOSED BROADBAND MMWAVE DOWN-CONVERSION MIXER ARCHITECTURE

Fig. 1 shows the proposed 24–40 GHz RF to 8 GHz IF down-conversion double-balanced mixer configuration. It comprises a transformer-coupled g_m-boosted CG G_m-stage, an S-to-D I-to-I capacitor-tuned RF coupled resonator, double-balanced active switching stages with a dual-band LO buffer, an IF coupled resonator load with gain equalization, and a wideband IF buffer with a D-to-S transformer-based balun. To meet the 5G NR FR2 specification, the RF input operating frequencies of 24.25–43.5 GHz is required in the mixer design. To support an inter-band carrier aggregation, it is very important that a single mixer covers all 5G NR FR2 frequencies. Considering two carrier component intra-band carrier aggregation scenario, the mixer should have 1 dB IF bandwidth of more than 0.8 GHz. The IF output frequency was set to 8 GHz.

The G_m-stage of the mixer employs the proposed wideband S-to-D I-to-I capacitor-tuned RF coupled resonator load to cover the 5G NR FR2 bands. Fig. 2(a) shows a conventional two-port I-to-V transformer-based RF coupled resonator. Unlike LC loads, the I-to-V coupled resonator load has transimpedance Z_{21} with two resonant peaks, tuned at two

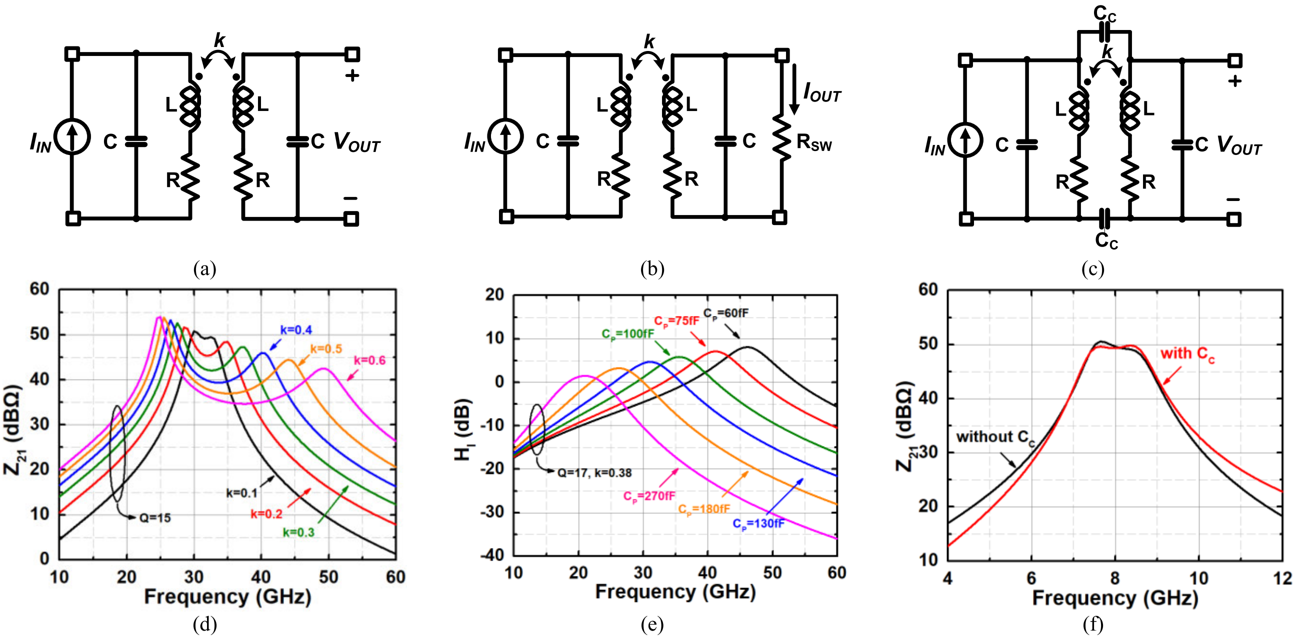

FIGURE 2. (a) Conventional I-to-V RF coupled resonator (b) proposed I-to-I RF coupled resonator (c) conventional I-to-V IF coupled resonator with gain equalization (d) simulated Z_{21} of I-to-V RF coupled resonator versus different k ($L = 0.23$ nH, $C = 120$ fF, $Q_L = 15$) (e) simulated H_I of I-to-I RF coupled resonator versus C ($k = 0.38$, $L = 0.23$ nH, $Q_L = 17$) (f) simulated Z_{21} of I-to-V IF coupled resonator with and without C_C ($k = 0.13$, $L = 1.23$ nH, $C = 320$ fF, $C_C = 50$fF, $Q_L = 12$).

different frequencies. The two resonant frequencies can be expressed as:

$$f_L = \frac{1}{2\pi\sqrt{L(1+k)C}} \quad \text{and}\ f_H = \frac{1}{2\pi\sqrt{L(1-k)C}}, \tag{1}$$

where L, C, and k are the inductance, capacitance, and magnetic coupling coefficient, respectively [20]. To simplify the analysis, a symmetric transformer structure is assumed. In other words, $L_1 = L_2 = L$, $C_1 = C_2 = C$, and $R_1 = R_2 = R$. Z_{21} at the resonant frequencies can be expressed as:

$$|Z_{21}|_{f=f_L} = \frac{L(1+k)}{2RC} \quad \text{and}\ |Z_{21}|_{f=f_H} = \frac{L(1-k)}{2RC}, \tag{2}$$

where R is the parasitic resistance of the inductor L. From (1), the separation between f_L and f_H can be tuned using k. Fig. 2(d) shows the simulated Z_{21} magnitude response versus different k. As k increases, the frequency separation increases. To connect the G_m-stage and I-to-I double-balanced active switching stages of the mixer, a modified I-to-I RF coupled resonator, shown in Fig. 2(b), is proposed. The transfer function of the I-to-I RF coupled resonator can be derived using the input impedance R_{SW} of the following switching stages, expressed as (3), as shown at the bottom of the page. From (3), we find that R_{SW} changes the frequency response of the I-to-I RF coupled resonator compared with the conventional I-to-V RF coupled resonator. The two resonant frequencies and Q-factors of the proposed I-to-I RF coupled resonator can be expressed as:

$$f_L = \frac{1}{2\pi\sqrt{L(1+k)C\frac{R_{SW}}{R+R_{SW}}}} \quad \text{and}\ f_H = \frac{1}{2\pi\sqrt{L(1-k)C}} \tag{4}$$

$$Q_1 \approx \sqrt{\frac{C(1+k)R_{SW}(R+R_{SW})}{L}} \quad \text{and}\ Q_2 = \frac{1}{R}\sqrt{\frac{L(1-k)}{C}}. \tag{5}$$

Assuming $R/R_{SW} \ll 1$ for a simple analysis, H_I at the resonant frequencies can be approximately expressed as:

$$|H_I|_{f=f_L} \approx \frac{L(1+k)}{2(R_{SW}RC+L)} \quad \text{and}\ |H_I|_{f=f_H} \approx \frac{L(1-k)}{2R_{SW}RC}. \tag{6}$$

As known from (4) and (5), the separation between f_L and f_H and Q_1 of the proposed I-to-I RF coupled resonator are lower than those of the conventional I-to-V RF coupled resonator. Consequently, the proposed I-to-I RF coupled resonator has wider frequency response. Fig. 2(e) shows the simulated H_I magnitude response of the proposed I-to-I RF coupled resonator. R_{SW} makes the magnitude response wider. If the capacitance C of the coupled resonator is tuned appropriately,

$$H_I(s) \approx \frac{I_{OUT}}{I_{IN}} \approx \frac{1}{R_{SW}} \frac{skL}{\left[s^2(1-k)LC + sRC + 1\right]\left[s^2(1+k)LC + s\left(RC + \frac{L}{R_{SW}}\right) + \left(1 + \frac{R}{R_{SW}}\right)\right]} \tag{3}$$

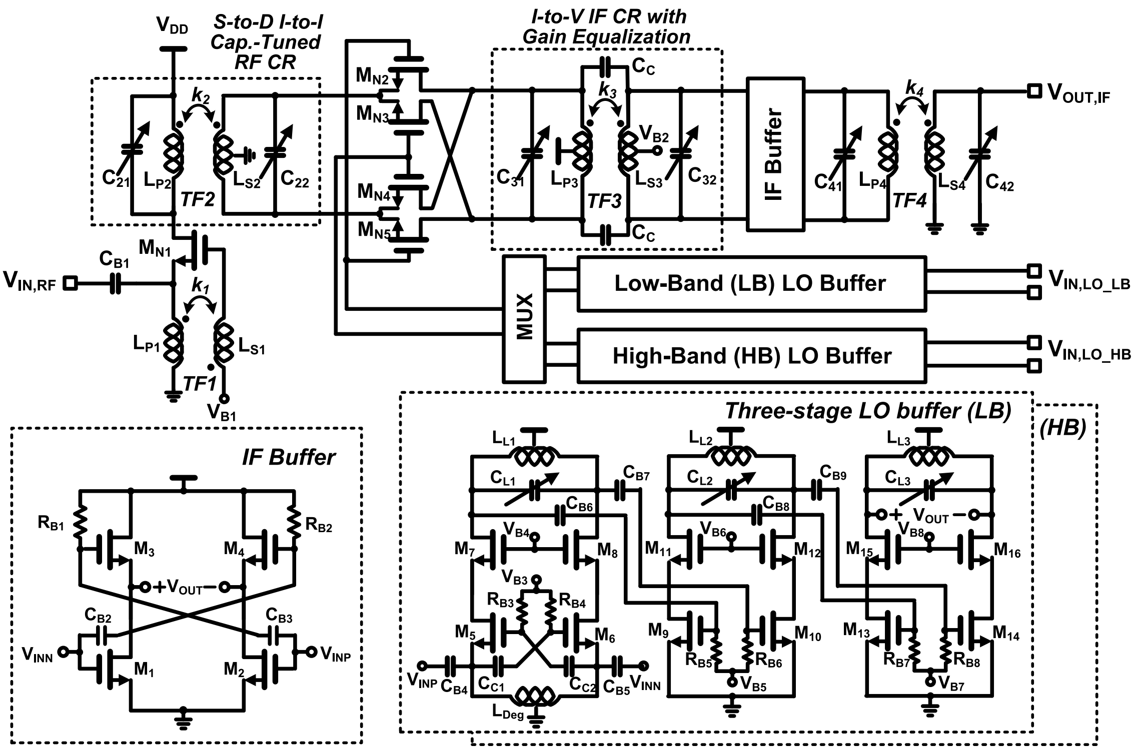

FIGURE 3. Simplified schematic of the proposed mmWave down-conversion mixer.

the proposed I-to-I RF coupled-resonator can provide sufficient current gain to cover the required 5G NR FR2 bands, as shown in Fig. 2(e). Because the conventional capacitor-tuned I-to-V RF coupled resonator cannot support all 5G NR FR2 bands due to the narrowband characteristic, the proposed capacitor-tuned I-to-I RF coupled resonator has a great advantage. Moreover, it performs S-to-D conversion. The required 1 dB IF bandwidth in the mixer output is $>$ 0.8 GHz. To meet this specification, a magnetically and electrically I-to-V IF coupled resonator load with low k, shown in Fig. 2(c), is employed after switching stages. It provides broadband and gain flatness characteristics. The capacitance C_C between the primary and secondary windings of the transformer can reduce the difference between the Z_{21} peak values at the two resonant frequencies [20]. Z_{21} of the magnetically and electrically coupled resonator load at the resonant frequencies can be expressed as:

$$|Z_{21}|_{f=f_L} = \frac{L(1+k)}{2R(C+C_C)} \quad \text{and} \quad |Z_{21}|_{f=f_H} = \frac{L(1-k)}{2RC}. \tag{7}$$

Fig. 2(f) shows the simulated Z_{21} of the I-to-V IF coupled resonator with and without C_C. C_C helps perform gain equalization. A parasitic capacitance between the two windings of the transformer was used to enhance the gain equalization of the IF coupled resonator through a thorough electro-magnetic (EM) simulation with the EMX tool. To drive a 50 Ω load, a wideband IF buffer with a transformer-based D-to-S balun was also used.

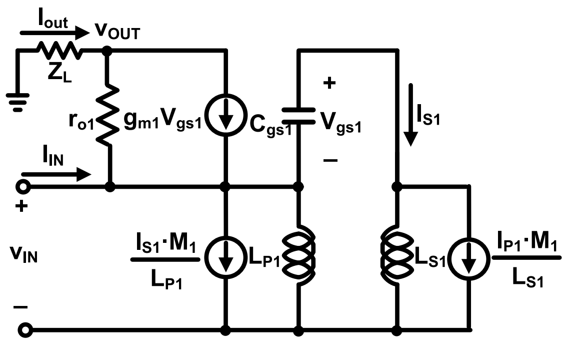

FIGURE 4. Small-signal model of the mixer G_m-stage.

III. CIRCUIT IMPLEMENTATION

This section describes the detailed circuit design of the broadband down-conversion double-balanced mixer for 5G NR FR2 applications. Fig. 3 shows the schematic of the proposed mmWave down-conversion mixer with a dual-band LO buffer.

A. TRANSFORMER-COUPLED g_m-BOOSTED COMMON-GATE G_m-STAGE

A transformer-coupled g_m-boosted CG configuration is used to boost the effective transconductance of the mixer G_m-stage. Transformer TF1 provides anti-phase operation between the

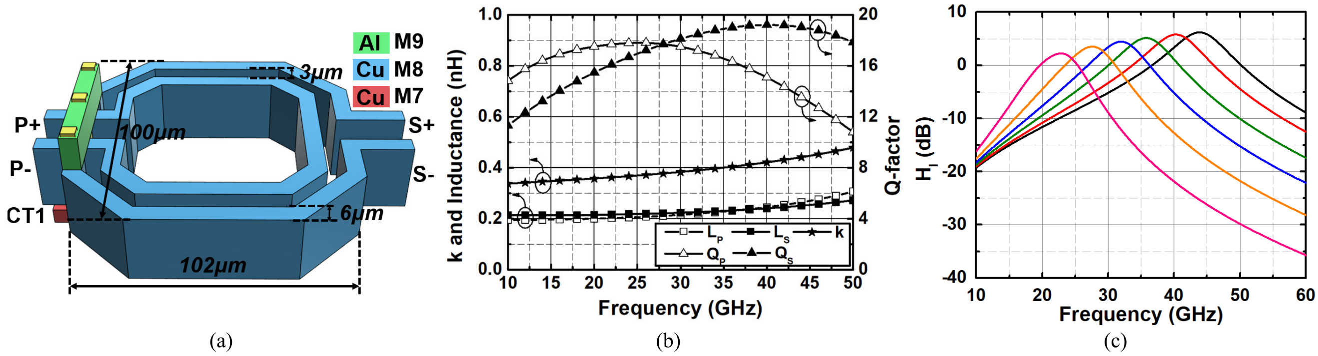

FIGURE 5. RF I-to-I coupled resonator: (a) transformer layout (b) inductance, Q and k of transformer (c) simulated H_I magnitude response of the I-to-I capacitor-tuned coupled resonator with a 4-bit capacitor array based on several capacitor codes.

gate and source terminals. A cascode transistor is not used to improve the noise performance at the cost of reverse isolation [21]. The input impedance and overall transconductance of the transformer-coupled g_m-boosted CG G_m-stage are analyzed using the small-signal model introduced in [22], which is shown in Fig. 4. For an intuitive and simple analysis, the effects of C_{gs} and channel-length modulation of M_{N1} are considered, while other parasitics and body effect are ignored. Using the Kirchhoff current law and Kirchhoff voltage law, the following equations can be derived.

$$I_{IN} + g_{m1}V_{gs1} + \frac{V_{OUT} - V_{IN}}{r_{o1}} = I_{S1} + \frac{M_1 I_{S1}}{L_{P1}} + \frac{V_{IN}}{sL_{P1}} \tag{8}$$

$$I_{S1} = \frac{V_{IN} + V_{gs1}}{sL_{S1}} + \frac{MI_{P1}}{L_{S1}} \tag{9}$$

$$I_{P1} = \frac{M_1 I_{S1}}{L_{P1}} + \frac{V_{IN}}{sL_{P1}} \tag{10}$$

$$V_{gs1} = -\frac{I_{S1}}{sC_{gs1}} \tag{11}$$

$$V_{OUT} = -Z_L I_{OUT} \tag{12}$$

$$I_{OUT} = g_{m1}V_{gs1} + \frac{V_{OUT} - V_{IN}}{r_{o1}} \tag{13}$$

Here, V_{gs1}, g_{m1}, r_{o1}, and C_{gs1} are the gate-to-source voltage, transconductance, output impedance, and gate-to-source capacitance of M_{N1}, respectively. Z_L is the load impedance. L_{P1}, L_{S1}, and M_1 are the self-inductances of the primary and secondary windings, and mutual inductance of transformer TF1, respectively. I_{P1} and I_{S1} are the currents flowing into the primary and secondary windings, respectively. From (8)–(13), the input admittance of the G_m-stage can be given as:

$$Y_{IN} = \frac{I_{IN}}{V_{IN}} = \frac{1}{sL_{P1}} + \frac{1}{r_{o1}}\left(1 - \frac{Z_L}{r_{o1} + Z_L}\right) + \frac{sC_{gs1}(1 + n_1 k_1)}{1 + s^2(1 - k_1^2)L_{S1}C_{gs1}} \times \left(\frac{g_{m1}}{sC_{gs1}}\left(1 - \frac{Z_L}{r_{o1} + Z_L}\right) + 1 + n_1 k_1\right) \tag{14}$$

where k_1 is a coupling coefficient ($k_1 = M_1/\sqrt{L_{P1}L_{S1}}$), and n_1 is the turns ratio ($n_1 = \sqrt{L_{P1}L_{S1}}$). When it is assumed that $g_{m1}r_{o1} \gg 1$, $Z_L/(r_{o1} + Z_L) \ll 1$, $\omega^2(1 - k_1^2)L_{S1}C_{gs1} \ll 1$, the input admittance of the G_m-stage can be simplified to

$$Y_{IN} \approx \frac{1}{sL_{P1}} + (1 + n_1 k_1)g_{m1} + s(1 + n_1 k_1)^2 C_{gs1}. \tag{15}$$

The overall transconductance of the G_m-stage is

$$|G_m| = \left|\frac{I_{OUT}}{V_{IN}}\right| = \frac{(1 + n_1 k_1)g_{m1}}{1 + s^2(1 - k_1^2)L_{S1}C_{gs1}} \frac{r_{o1}}{r_{o1} + Z_L} + \frac{1}{r_{o1} + Z_L} \approx (1 + n_1 k_1)g_{m1}. \tag{16}$$

The transformer-coupled configuration increases the effective transconductance by $(1 + n_1 k_1)$.

B. SWITCHING STAGE WITH DUAL-BAND LO BUFFER

The double-balanced active switching stage, where the transistors of M_{N2}, M_{N3}, M_{N4}, and M_{N5} are switched between the saturation and cut-off regions, are driven by a dual-band LO buffer. The required operating frequency range of the LO buffer is 16.25–35.5 GHz because the mixer has 24.25–43.5 GHz RF and 8 GHz IF. Since it is difficult to design a broadband amplifier that covers such a wide frequency range, the LO buffer is designed to be divided into two bands to obtain sufficient voltage gain stably. Fig. 3 shows the proposed dual-band LO buffer. In each band, a three-stage LO buffer is employed, which is composed of a cross-coupled CG amplifier, and two common-source amplifiers. All the amplifiers adopt cascode transistors to enhance the voltage gains. Because adjacent inductors can influence each other, L_{Deg}, L_{L1}, L_{L2}, and L_{L3} were co-designed through a thorough EM simulation. Low-band and high-band LO signals are selected through the MUX and supplied to the switching transistor. The simulated voltage gains of the LO buffers including the routing line and MUX exceed 18 dB for all operating frequencies. When an LO input signal with $P_{LO} = -10$ dBm is applied, the LO buffer can stably drive the switching stages to achieve the maximum conversion gain and minimum NF of the mixer.

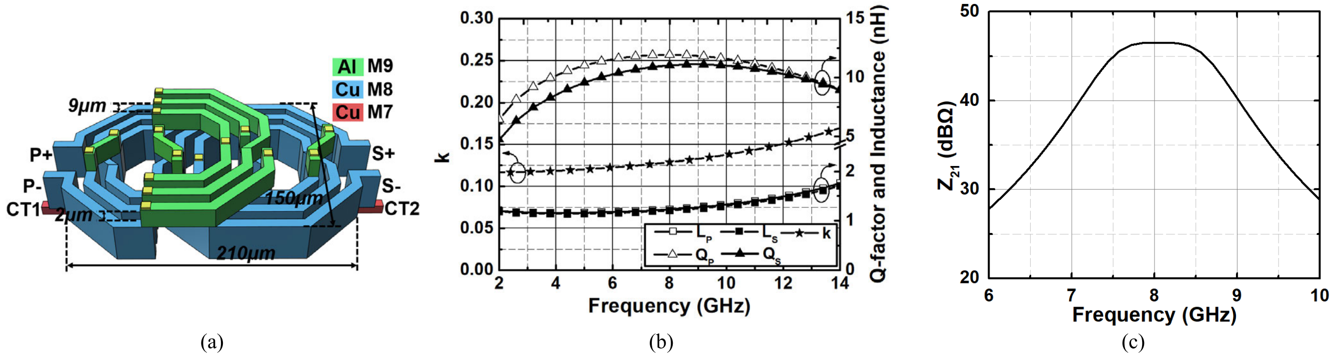

FIGURE 6. IF I-to-V coupled resonator: (a) transformer layout (b) inductance, Q and k of transformer (c) simulated Z_{21} magnitude response of the I-to-V coupled resonator with a 4-bit capacitor array.

C. RF AND IF COUPLED RESONATORS

The k of the transformer for the I-to-I RF coupled resonator was set to 0.38 to provide a broadband frequency response. Fig. 5(a) and (b) illustrate the layout and simulated parameters of the designed transformer, respectively. The EM simulated $L_P/L_S/Q_P/Q_S/k$ values at 24 and 40 GHz are 0.21 nH/0.22 nH/17.8/16.7/0.37 and 0.25 nH/0.24 nH/15.1/19.2/0.42, respectively. In addition, by adopting a 4-bit digitally-controlled capacitor array, the resonant peak of the RF coupled resonator can be tuned based on the operating band. The simulated H_I magnitude responses of the implemented broadband S-to-D I-to-I capacitor-tuned RF coupled resonator with the 4-bit capacitor array based on several codes are depicted in Fig. 5(c). The designed RF coupled resonator covers all 5G NR FR2 operating bands.

Fig. 6(a) and (b) show the layout and simulated parameters of the transformer for the I-to-V IF coupled resonator load, respectively. To obtain a low k, the overlap between the primary and secondary windings is minimized. The EM simulated L_P, L_S, Q_P, Q_S, and k at 8 GHz are 1.23 nH, 1.21 nH, 11.9, 11, and 0.13, respectively. A parasitic capacitance between the two windings of the transformer was used as C_C to enhance the gain equalization of the IF coupled resonator. The optimal transformer was designed through numerous trials and errors through a thorough EM simulation by adjusting the width, layer, and spacing of the metal and overlapping area of the two windings of the transformer. Fig. 6(c) shows the simulated Z_{21} magnitude response of the IF coupled resonator employing gain equalization with the 4-bit capacitor array. When $k = 0.13$, the IF load has the 1 dB bandwidth of more than 0.8 GHz. C_{31} and C_{32} can be tuned using 4-bit digitally controlled signals to compensate for the center frequency variation due to the process, voltage, and temperature variations.

D. WIDEBAND IF BUFFER WITH BALUN

A wideband IF buffer with a transformer-based 1:1 balun is used to drive the single-ended 50 Ω. As shown in Fig. 3, the topology of the IF buffer involves a CS amplifier and cross-stacked source-follower [23]. The gain of this combined topology can be expressed as:

$$A_{VBF} \approx g_{m1}\left(\frac{1}{g_{m3}}||r_{o1}||r_{o3}||\frac{R_L}{2}\right)+\frac{(r_{o1}||r_{o3}||\frac{R_L}{2})}{\frac{1}{g_{m3}}+(r_{o1}||r_{o3}||\frac{R_L}{2})}, \tag{17}$$

where g_{mi} and r_{oi} are the transconductance and output impedance of M_i, respectively, and R_L is the load impedance of the buffer, which is close to 50 Ω. When $g_{m1} = g_{m3} = g_{mBF}, r_{o1} = r_{o3} = r_{oBF}, g_{mBF}r_{oBF} \gg 1$, the gain is simplified to $2g_{mBF}R_L/(2 + g_{mBF}R_L)$. From (17), we find that the gain of the current-reused IF buffer is almost twice than that of the conventional source follower.

E. CONVERSION GAIN

Considering the source resistance R_S and input impedance matching condition of $(1 + n_1k_1)g_{m1}R_S = 1$, the conversion gain of the proposed down-conversion mixer can be approximated as

$$A_{VMixer} \approx \frac{1}{\pi}(1+n_1k_1)g_{m1}H_I(s)Z_{21IFCR}A_{VBF}n_4k_4, \tag{18}$$

where $Z_{21IFCR} = L_{P3}(1 + k_3)/2R_{LP3}C_{31}$, $A_{VBF} = 2g_{mBF}R_L/(2 + g_{mBF}R_L)$, and R_{LP3} is the parasitic resistance of L_{P3} in TF3.

F. NOISE ANALYSIS

The noise sources were assumed to be uncorrelated to each other. For simplicity, the body effect, channel-length modulation, and induced gate noise were also ignored. When a voltage source V_S with a source impedance R_S is applied to the source of M_{N1}, the total noise factor of the proposed down-conversion mixer can be expressed as:

$$\begin{aligned} F &\approx 1+\frac{V_{Gm}^2+V_{SW}^2+V_{IFCR}^2+V_{IFBF}^2}{4kTR_SA_{VMixer}^2} \\ &= 1+EF_{Gm}+EF_{SW}+EF_{IFCR}+EF_{IFBF} \end{aligned} \tag{19}$$

where EF is the excess noise factor used to quantify the noise contribution of each sub-block to the overall noise factor F, k is the Boltzmann's constant, T is the absolute temperature, A_{VMixer} is the conversion gain from the voltage source V_S

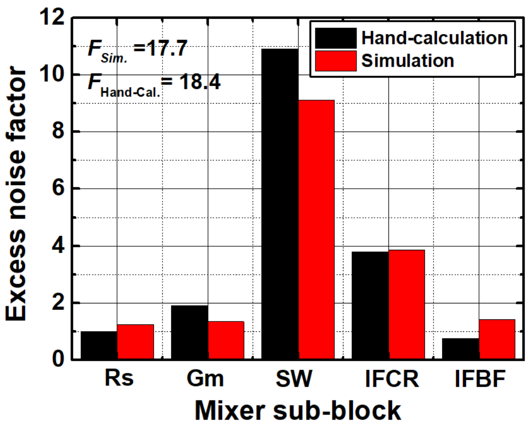

FIGURE 7. Simulated excess noise factor of the mixer sub-block at 28 GHz RF and 8 GHz IF (under the condition of input impedance match, g_{m1} = 35 mS, n_1 = 0.63, k_1 = 0.47, n_2 = 1, k_2 = 0.38, n_3 = 1, k_3 = 0.13, n_4 = 0.94, k_4 = 0.71, g_{mBF} = 40 mS, and R_L = 50 Ω.).

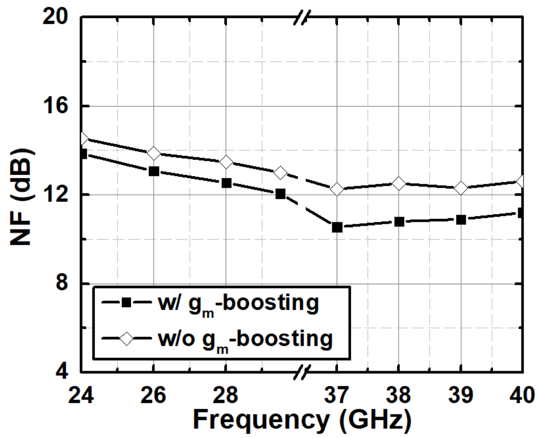

FIGURE 8. Simulated NFs of the mixer with transformer-coupled g_m-boosted CG G_m-stage and basic CG G_m-stage.

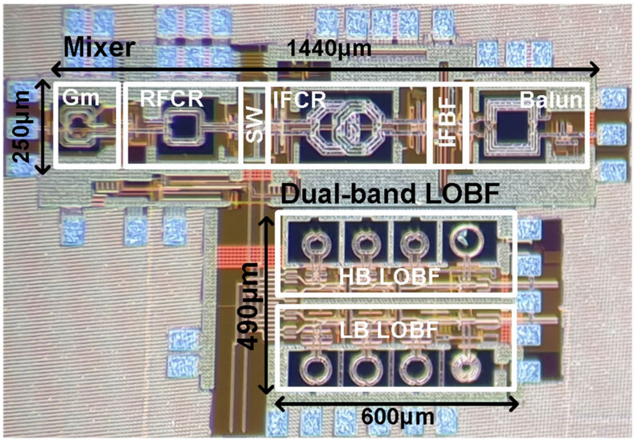

FIGURE 9. Chip photograph.

to the output $V_{OUT,IF}$, and V_{GM}^2, V_{SW}^2, V_{IFCR}^2, and V_{IFBF}^2 represent the output-referred noise voltages generated by G_m-stage, switching stages, IF coupled resonator load, and IF buffer, respectively [24]. To simplify the analysis, the parallel parasitic resistance of the I-to-I RF coupled resonator seen to the following switching stages is assumed to be much higher than the input impedance of the switching stages. The RF coupled resonator can remove the white noises in the image band and all its odd harmonics to some extent; therefore, their effect is ignored. The excess noise factors with an input impedance match condition of $(1 + n_1k_1)g_{m1}R_S = 1$ can be derived as follows:

$$EF_{Gm} \cong \frac{1}{4kTR_S}\frac{4kT\gamma g_{m1}}{((1+n_1k_1)g_{m1})^2} = \frac{\gamma}{1+n_1k_1} \tag{20}$$

$$\begin{aligned} EF_{SW} &\cong \frac{1}{4kTR_S}\frac{4\times 4kT\gamma\frac{I_B}{\pi A}}{\left(\frac{1}{\pi}(1+n_1k_1)g_{m1}H_I\right)^2} \\ &= \frac{4\pi\gamma I_B}{A(1+n_1k_1)g_{m1}H_I^2} \end{aligned} \tag{21}$$

$$\begin{aligned} EF_{IFCR} &\cong \frac{1}{4kTR_S}\frac{4kT\frac{L_{P3}(1+k_3)}{2R_{LP3}C_{31}}}{\left(\frac{1}{\pi}(1+n_1k_1)g_{m1}H_I\frac{L_{P3}(1+k_3)}{2R_{LP3}C_{31}}\right)^2} \\ &= \frac{2\pi^2R_{LP3}C_{31}}{(1+n_1k_1)g_{m1}H_I^2(1+k_3)L_{P3}} \end{aligned} \tag{22}$$

$$\begin{aligned} EF_{IFBF} &\cong \frac{1}{4kTR_S}\frac{\frac{4kT\gamma}{g_{mBF}} + kT\gamma R_L\left(\frac{2+g_{mBF}R_L}{g_{mBF}R_L}\right)^2}{\left(\frac{1}{\pi}(1+n_1k_1)g_{m1}H_I\frac{L_{P3}(1+k_3)}{2R_{LP3}C_{31}}\right)^2} \\ &= \frac{\pi^2\gamma R_{LP3}^2C_{31}^2}{(1+n_1k_1)g_{m1}H_I^2L_{P3}^2(1+k_3)^2g_{mBF}} \\ &\quad\times\left(4+\frac{(2+g_{mBF}R_L)^2}{R_L}\right) \end{aligned} \tag{23}$$

where A is the LO amplitude, and I_B is the dc bias current of the switching stage [25]. From (20)–(23), the noise factor of the proposed down-conversion mixer can be expressed as:

$$\begin{aligned} F &\approx 1 + \frac{\gamma}{1+n_1k_1} + \frac{4\pi\gamma I_B}{A(1+n_1k_1)g_{m1}H_I^2} \\ &\quad + \frac{2\pi^2R_{LP3}C_{31}}{(1+n_1k_1)g_{m1}H_I^2(1+k_3)L_{P3}} \\ &\quad + \frac{\pi^2\gamma R_{LP3}^2C_{31}^2}{(1+n_1k_1)g_{m1}H_I^2L_{P3}^2(1+k_3)^2g_{mBF}} \\ &\quad \times\left(4+\frac{(2+g_{mBF}R_L)^2}{R_L}\right) \end{aligned} \tag{24}$$

Fig. 7 shows the simulated excess noise factor of the mixer sub-block at 28 GHz RF and 8 GHz IF under the condition of input impedance match, g_{m1} = 35 mS, n_1 = 0.63, k_1 = 0.47, n_2 = 1, k_2 = 0.38, n_3 = 1, k_3 = 0.13, n_4 = 0.94, k_4 = 0.71, g_{mBF} = 40 mS, and R_L = 50 Ω. As expected, the excess noise factor of the switching stages has the most dominant effect in determining the overall NF performance. Fig. 8 shows the simulated NFs of the mixer with the transformer-coupled g_m-boosted CG G_m-stage and basic CG G_m-stage. By employing the transformer-coupled

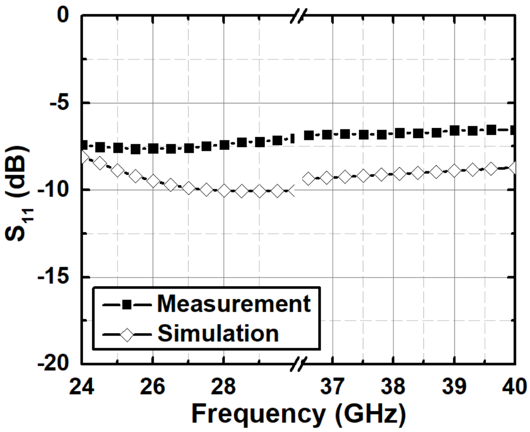

FIGURE 10. Measured and simulated S_{11}.

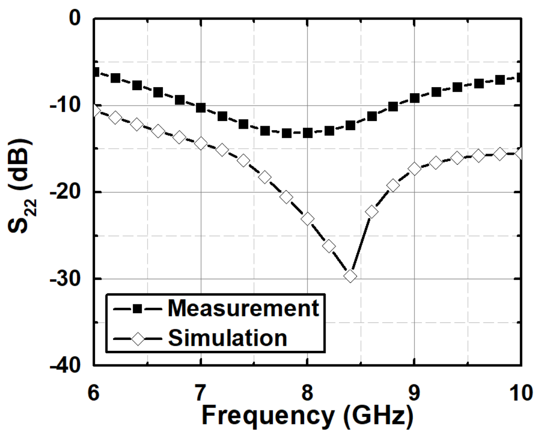

FIGURE 11. Measured and simulated S_{22}.

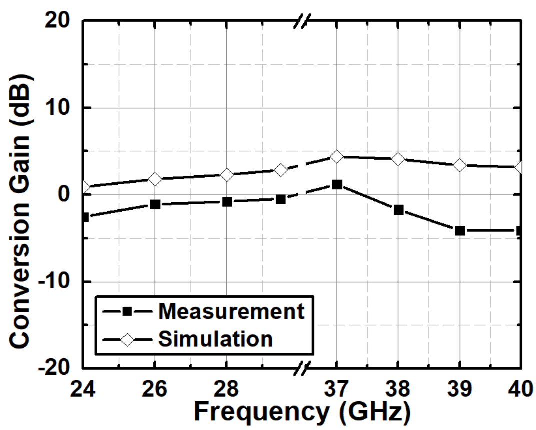

FIGURE 12. Measured and simulated conversion gains.

g_m-boosted CG G_m -stage, the mixer achieves 0.7-1.7 dB NF improvement.

IV. EXPERIMENTAL RESULTS

The proposed mmWave broadband down-conversion double-balanced mixer with the dual-band LO buffer for 5G NR FR2 applications was implemented in a 40 nm CMOS process.

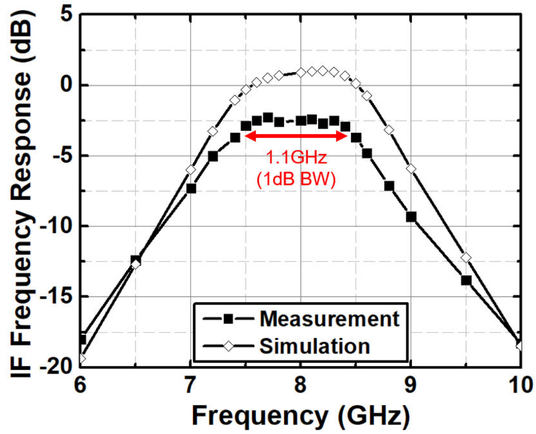

FIGURE 13. Measured and simulated IF frequency response with an RF frequency of 24.25 GHz.

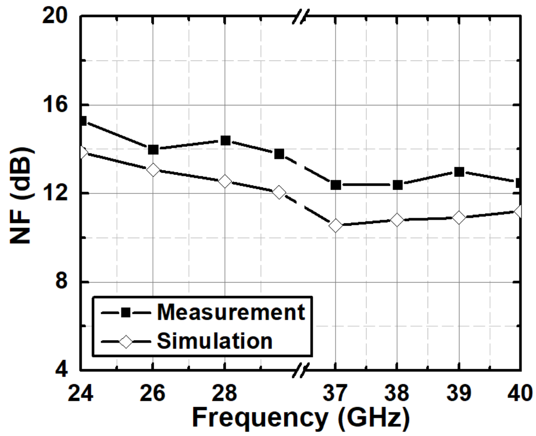

FIGURE 14. Measured and simulated NF.

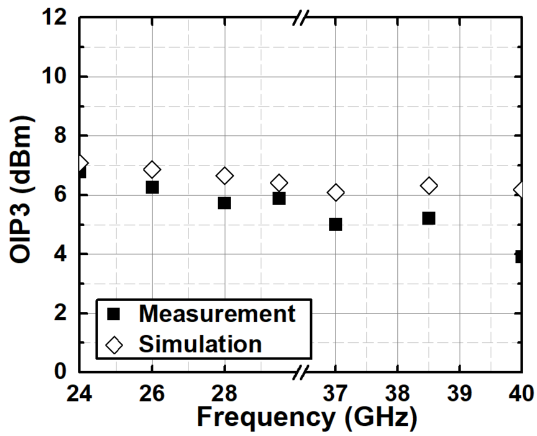

FIGURE 15. Measured and simulated OIP3.

The chip photograph is demonstrated in Fig. 9. The effective active areas of the mixer and LO buffer without the bond pads are 0.36 and 0.294 mm^2, respectively. The power consumptions of the mixer and dual-band LO buffer are 17.6 and 10.7 mW with a nominal supply voltage of 1.1 V, respectively. The power consumptions of the G_m-stage, double- balanced switching stages, and IF buffer in the implemented mixer are 5.83, 2.07, and 9.7 mW, respectively. The measurement of

TABLE 1. Performance summaries of the proposed mmWave down-conversion mixer and comparison with previous works.

	Mixer Architecture	Process	RF Frequency [GHz]	IF Frequency [GHz]	Conversion Gain [dB]	SSB NF [dB]	OIP3 [dBm]	P1dB [dBm]	Pdc [mW]	VDD [V]	Area [mm^2]
JSSC 2018 [2]	DBM[1)] + Current-bleeding	28-nm CMOS	25.8–28	0	−2–5[3)]	14–19.9[3)]	1.2[3)4)]	−12.6[3)]	N.A.	1.05	N.A.
MWCL 2015 [11]	DBM with MGTR	45-nm SOI CMOS	31	12	3.4	9.5	21.4	−4.2	21.2	1.5	0.8
MWCL 2018 [12]	DBM with Distributed DS	180-nm CMOS	23–25	N.A.	−4.4	N.A.	18.6[4)]	−11	16	2	0.72
MWCL 2021 [13]	Bidirectional DBM + IF Buffer	90-nm CMOS	25–31	1	−3.28	14.32	N.A.	−13	6.4	1.2	0.52
ACCESS 2019 [14]	DBM + IF Buffer	130-nm CMOS	23–25	N.A.	26.1	7.7	N.A.	−17.8	16.8	1.5	0.96
MWCL 2012 [15]	SBM[2)] + IF Buffer + LO Buffer	90-nm CMOS	57–66	1	12	15	−0.5	−23	8.8	1.2	0.24
TCASII 2013 [16]	SBM + IF Buffer	130-nm CMOS	20–26	0.3	9.15	3.61-5	5.75	−13	23.2	N.A.	0.49
MWCL 2015 [17]	4 x Subharmonic mixer + IF Buffer	65-nm CMOS	79–110	1	8	15.5	8.4[4)]	−9.2	17	1.5	0.37
MWCL 2017 [18]	DBM + IF Balun + LO Buffer	65-nm CMOS	57–66	12	5.6	11	12.4	−7	18	1	0.22
This Work	DBM + IF Buffer + Balun + LO Buffer	40-nm CMOS	24–40	8	−4.1–1.2	12.4–15.3	4–6.8	−0.5	28.3	1.1	0.654

1) DBM: double-balanced mixer 2) SBM: single-balanced mixer 3) Simulation results 4) OIP3 = IIP3 + Gain

the mixer was performed using an on-wafer probing. The RF input and IF output of the mixer were probed with ground-signal-ground (GSG) RF probes, and the LO signal was provided through a bonding wire on the test PCB board. Supply voltages and SPI control signals were also provided from the PCB board.

The measured and simulated S_{11} and S_{22} of the down-conversion mixer are depicted in Fig. 10 and 11, respectively. The measured S_{11} is less than -6.5 in the entire frequency range of 24–40 GHz, and the measured S_{22} is less than -10 dB at an IF frequency of 8 GHz. When it is actually used in the receiver, the S_{11} characteristic is expected to improve because there is no test pad for measuring the mixer input. Fig. 12 shows the measured and simulated conversion gains of the down-conversion mixer. The measured conversion gain in the 24–30 and 37–40 GHz frequency bands are obtained from -2.5 to -0.46 dB and -4.1 to 1.2 dB, respectively. The frequency response of the mixer in the IF frequency range is illustrated in Fig. 13. The measured 1 dB bandwidth of the mixer IF output is more than 1.1 GHz. The proposed IF coupled resonator load with gain equalization improves the gain flatness and bandwidth. As shown in Fig. 14, the measured NF in the 24–30 and 37−40 GHz frequency bands are obtained from 13.8 to 15.3 dB and 12.4 to 13 dB, respectively. Fig. 15 depicts the measured and simulated OIP3. The two-tone test conditions for the IIP3 are $f_1 = f_{IMD3} + 10$ MHz and $f_2 = f_{IMD3} + 20$ MHz, where f_{IMD3} is the third-order intermodulation distortion (IMD3) frequency. The measured OIP3 in the 24–30 and 37–40 GHz frequency bands are obtained from 5.73 to 6.8 dB and 4 to 5.2 dB, respectively. The proposed down-conversion mixer can also support n259 (39.5–43.5 GHz) based on the simulation results with parasitic extraction. However, it has been measured up to 40 GHz because of the limitation of the measurement equipment.

Table 1 summarizes and compares the performances of the implemented mmWave down-conversion mixer with previous state-of-the-arts. This work achieves the best performance in terms of the operating frequency range. It can cover all 5G FR2 bands.

V. CONCLUSION

A broadband mmWave down-conversion double-balanced mixer employing RF and IF coupled resonators with a dual-band three-stage LO buffer was implemented for 5G NR FR2 applications through a 40 nm CMOS process. In the proposed mixer architecture, the transformer-coupled g_m-boosted CG G_m-stage improved the noise performance, and the I-to-I capacitor-tuned RF coupled resonator and I-to-V IF coupled resonator with gain equalization provided broadband frequency characteristics such as an RF operating frequency range of 24–40 GHz and a 1 dB IF bandwidth of more than 0.8 GHz. The proposed wideband down-conversion mixer topology can serve as an effective candidate in 5G NR FR2 transceivers employed in mobile phones.

REFERENCES

[1] J. D. Dunworth, A. Homayoun, B.-H. Ku, Y.-C. Ou, K. Chakraborty, G. Liu, T. Segoria, J. Lerdworatawee, J. W. Park, H.-C. Park, H. Hedayati, D. Lu, P. Monat, K. Douglas, and V. Aparin, "A 28 GHz bulk-CMOS dual-polarization phased-array transceiver with 24 channels for 5G user and basestation equipment," in *IEEE ISSCC Dig. Tech. Papers*, San Francisco, CA, USA, Feb. 2018, pp. 70–72.

[2] H. Kim, B. Park, S. Song, T. Moon, S. Kim, J. Kim, J. Chang, and Y. Ho, "A 28-GHz CMOS direct conversion transceiver with packaged 2×4 antenna array for 5G cellular system," *IEEE J. Solid-State Circuits*, vol. 53, no. 5, pp. 1245–1259, May 2018.

[3] S. Mondal, R. Singh, A. I. Hussein, and J. Paramesh, "A 25–30 GHz fully-connected hybrid beamforming receiver for MIMO communication," *IEEE J. Solid-State Circuits*, vol. 53, no. 5, pp. 1275–1287, May 2018.

[4] B. Jann, G. Chance, A. G. Roy, A. Balakrishnan, N. Karandikar, T. Brown, X. Li, B. Davis, J. L. Ceballos, N. Tanzi, K. Hausmann, H. Yoon, Y.-L. Huang, A. Freiman, B. Geren, P. Pawliuk, and W. Ballantyne, "A 5G sub-6 GHz zero-IF and mm-wave IF transceiver with MIMO and carrier aggregation," in *IEEE ISSCC Dig. Tech. Papers*, Feb. 2019, pp. 352–354.

[5] J. Pang *et al.*, "A 28 GHz CMOS phased-array beamformer utilizing neutralized bi-directional technique supporting dual-polarized MIMO for 5G NR," in *IEEE ISSCC Dig. Tech. Papers*, San Francisco, CA, USA, Feb. 2019, pp. 352–354.

[6] M.-Y. Huang and H. Wang, "A 27-to-41 GHz MIMO receiver with N-input-N-output using scalable cascadable autonomous array-based high-order spatial filters for instinctual full-FoV multi-blocker/signal management," in *IEEE ISSCC Dig. Tech. Papers*, San Francisco, CA, USA, Feb. 2019, pp. 346–348.

[7] S. Mondal and J. Paramesh, "A reconfigurable 28-/37-GHz MMSE-adaptive hybrid-beamforming receiver for carrier aggregation and multi-standard MIMO communication," *IEEE J. Solid-State Circuits*, vol. 54, no. 5, pp. 1391–1406, May 2019.

[8] S. Mondal, L. R. Carley, and J. Paramesh, "A 28/37 GHz scalable, reconfigurable multi-layer hybrid/digital MIMO transceiver for TDD/FDD and full-duplex communication," in *IEEE ISSCC Dig. Tech. Papers*, San Francisco, CA, USA, Feb. 2020, pp. 82–84.

[9] H.-C. Park *et al.*, "A 39 GHz-band CMOS 16-channel phased-array transceiver IC with a companion dual-stream IF transceiver IC for 5G NR base-station applications," in *IEEE ISSCC Dig. Tech. Papers*, San Francisco, CA, USA, Feb. 2020, pp. 76–78.

[10] B. Sadhu, Y. Tousi, J. Hallin, S. Sahl, S. Reynolds, Ö. Renström, K. Sjögren, O. Haapalahti, N. Mazor, B. Bokinge, G. Weibull, H. Bengtsson, A. Carlinger, E. Westesson, J.-E. Thillberg, L. Rexberg, M. Yeck, X. Gu, D. Friedman, and A. V. Garcia, "A 28 GHz 32-element phased-array transceiver IC with concurrent dual polarized beams and 1.4 degree beam-steering resolution for 5G communication," in *IEEE ISSCC Dig. Tech. Papers*, San Francisco, CA, Feb. 2017, pp. 128–130.

[11] C.-L. Wu, C. Yu, and K. K. O, "Amplification of nonlinearity in multiple gate transistor millimeter wave mixer for improvement of linearity and noise figure," *IEEE Microw. Wireless Compon. Lett.*, vol. 25, no. 5, pp. 310–312, May 2015.

[12] H. Lin, Y. Lin, and H. Wang, "A high linearity 24-GHz down-conversion mixer using distributed derivative superposition technique in 0.18-μm CMOS Process," *IEEE Microw. Wireless Compon. Lett.*, vol. 28, no. 1, pp. 49–51, May 2018.

[13] Y.-T. Chang and K.-Y. Lin, "A 28-GHz bidirectional active Gilbert-cell mixer in 90-nm CMOS," *IEEE Microw. Wireless Compon. Lett.*, vol. 31, no. 5, pp. 473–476, May 2021.

[14] Y. Peng, J. He, H. Hou, H. Wang, S. Chang, Q. Huang, and Y. Zhu, "A K-band high-gain and low-noise folded CMOS mixer using current-reuse and cross-coupled techniques," *IEEE Access*, vol. 7, pp. 133218–133226, 2019.

[15] C. W. Byeon, J. J. Lee, I. S. Song, and C. S. Park, "A 60 GHz current-reuse LO-boosting mixer in 90 nm CMOS," *IEEE Microw. Wireless Compon. Lett.*, vol. 22, no. 3, pp. 135–137, Mar. 2012.

[16] S. Kong, C. Kim, and S. Hong, "A K-band UWB low-noise CMOS mixer with bleeding path G_m-boosting technique," *IEEE Trans. Circuits Syst. II, Exp. Briefs*, vol. 60, no. 3, pp. 117–121, Mar. 2013.

[17] T. Huang, X. Yi, C. Boon, X. He, G. Feng, W. Lim, and X. Zhu, "A CMOS W-band 4X quasi-subharmonic mixer," *IEEE Microw. Wireless Compon. Lett.*, vol. 25, no. 6, pp. 385–387, Jun. 2015.

[18] C. Choi, J. H. Son, O. Lee, and I. Nam, "A +12-dBm OIP3 60-GHz RF downconversion mixer with an output-matching, noise- and distortion-canceling active balun for 5G applications," *IEEE Microw. Wireless Compon. Lett.*, vol. 27, no. 3, pp. 284–286, Jun. 2017.

[19] N. Mazor, B. Sheinman, O. Katz, R. Levinger, E. Bloch, R. Carmon, R. Ben-Yishay, and D. Elad, "Highly linear 60-GHz SiGe Downconversion/Upconversion mixers," *IEEE Microw. Wireless Compon. Lett.*, vol. 27, no. 4, pp. 401–403, Apr. 2017.

[20] V. Bhagavatula, T. Zhang, A. Suvarna, and J. Rudell, "An ultra-wideband IF millimeter-wave receiver with a 20 GHz channel bandwidth using gain-equalized transformers," *IEEE J. Solid-State Circuits*, vol. 51, no. 2, pp. 323–331, Feb. 2016.

[21] N. Li, K. Okada, T. Suzuki, T. Hirose, and A. Matsuzawa, "A three-stage 60 GHz CMOS LNA using dual noise-matching technique for 5dB NF," in *Proc. Asia–Pacific Microw. Conf.*, Dec. 2008, pp. 1–4.

[22] J. R. Long, "Monolithic transformers for silicon RF IC design," *IEEE J. Solid-State Circuits*, vol. 35, no. 9, pp. 1368–1382, Sep. 2000.

[23] S. Kim and K. Kwon, "A 50-MHz–1-GHz 2.3-dB NF noise-cancelling balun-LNA employing a modified current-bleeding technique and balanced loads," *IEEE Trans. Circuits Syst. I, Reg. Papers*, vol. 66, no. 2, pp. 546–554, Feb. 2019.

[24] B. Razavi, *RF Microelectronics*, 2nd ed. New York, NY, USA: Prentice-Hall, 2012.

[25] H. Darabi and A. A. Abidi, "Noise in RF-CMOS mixers: A simple physical model," *IEEE J. Solid-State Circuits*, vol. 35, no. 1, pp. 15–25, Jan. 2000.

DONGGU LEE (Student Member, IEEE) received the B.S. and M.S. degrees from the Department of Electronics Engineering, Kangwon National University, Chuncheon, South Korea, in 2019 and 2021, respectively, where he is currently pursuing the Ph.D. degree with the Department of Electronics Engineering. His research interests include CMOS mmWave/RF/analog integrated circuits and RF system design for wireless communications.

He was a recipient of Korean Intellectual Property Office (KIPO) Commissioner Award and ADT Special Award for Korea Semiconductor Design Competition, in 2018 and 2019, and 3rd Award for 11th ETNEWS ICT Best Paper Award, in 2019.

MYUNGHUN LEE (Member, IEEE) received the integrated B.S. and M.S. degrees from the Department of Electronics Engineering, Kangwon National University, Chuncheon, South Korea, in 2021. In 2021, he joined Samsung Electronics Company Ltd., Hwaseong-si, South Korea. His research interests include CMOS mmWave/RF/analog integrated circuits and RF system design for wireless communications.

He was a recipient of Ministry of Trade, Industry and Energy Award for Korea Semiconductor Design Competition, in 2019, and 3rd Award for 11th ETNEWS ICT Best Paper Award, in 2019.

BEOMYU PARK (Member, IEEE) received the integrated B.S. and M.S. degrees from the Department of Electronics Engineering, Kangwon National University, Chuncheon, South Korea, in 2021. In 2021, he joined Samsung Electronics Company Ltd., Hwaseong-si, Gyeonggi-Do, South Korea. His research interests include CMOS mmWave/RF/analog integrated circuits and RF system design for wireless communications.

He was a recipient of Ministry of Trade, Industry and Energy Award for Korea Semiconductor Design Competition, in 2019, and 3rd Award for 11th and 12th ETNEWS ICT Best Paper Award, in 2019 and 2020.

EUNJU SONG (Student Member, IEEE) received the integrated B.S. and M.S. degrees from the Department of Electronics Engineering, Kangwon National University, Chuncheon, South Korea, in 2021.

In 2021, she joined NICE Information Company Ltd., Seoul, South Korea. Her research interests include CMOS mmWave/ RF/analog integrated circuits and RF system design for wireless communications.

KYUDO LEE (Student Member, IEEE) received the B.S. degree from the Department of Electronics Engineering, Kangwon National University, Chuncheon, South Korea, in 2021, where he is currently pursuing the M.S. degree with the Department of Electronics Engineering.

His research interests include CMOS mmWave/RF/analog integrated circuits and RF system design for wireless communications.

JEONGWOO LEE (Member, IEEE) received the B.S. and M.S. degrees in electronics engineering and the Ph.D. degree in electrical engineering from Seoul National University, Seoul, South Korea, in 1994, 1996, and 2000, respectively.

In 2000, he joined GCT Semiconductor Inc., San Jose, CA, USA, as a Founder Engineer, where he is currently the Senior Director of Engineering. His research interest includes CMOS transceiver circuitry for highly integrated radio applications. He has been involved with the development of various CMOS RF chip sets for W-CDMA, DMB, WiMAX, and LTE. He is currently leading the development of 5G NR RF products.

JUNGHWAN HAN (Member, IEEE) was born in Daegu, South Korea, in 1977. He received the B.S. degree (Hons.) from Inha University, Incheon, South Korea, in 2002, the M.S. degree from the University of Michigan, Ann Arbor, in 2004, and the Ph.D. degree from the University of Texas at Austin, in 2007, all in electrical engineering.

From 2008 to 2010, he was with Qualcomm Inc., Santa Clara, CA, USA, where he designed and developed various CMOS RF front-end circuits for WLAN and GPS applications. From 2010 to 2017, he was a Senior Engineer and a Principle Engineer at Samsung Electronics Company Ltd., Hwasung, South Korea. He has been involved with the development of CMOS transceivers for several cellular applications, including GSM, WCDMA, LTE, and 5G standards. Since 2017, he has been joining the Department of Radio Science and Information Communication Engineering, Chungnam National University, Daejeon, South Korea, where he is currently an Assistant Professor. His research interests include low-power analog and RF integrated circuit and system design for wired and wireless communication systems.

Dr. Han was a recipient of the Best Paper Award from IEEE Journal of Solid-State Circuits, in 2008.

KUDUCK KWON (Senior Member, IEEE) received the B.S. and Ph.D. degrees in electrical engineering and computer science from the Korea Advanced Institute of Science and Technology (KAIST), Daejeon, South Korea, in 2004 and 2009, respectively.

His Ph.D. research concerned digital TV tuners and dedicated short-range communication (DSRC) systems. From 2009 to 2010, he was a Postdoctoral Researcher with KAIST, where he studied a surface acoustic wave (SAW)-less receiver architectures and developed 5.8GHz RF transceivers for DSRC applications. From 2010 to 2014, he was a Senior Engineer with Samsung Electronics Company Ltd., Suwon, South Korea, where he has been involved with studies of the SAW-less software-defined receivers and development of CMOS transceivers for 2G/3G/4G cellular applications and receivers for universal silicon tuners. In 2014, he joined the Department of Electronics Engineering, Kangwon National University, Chuncheon, South Korea, where he is currently an Associate Professor. His research interests include CMOS mmWave/RF/analog integrated circuits and RF system design for wireless communications.